


Expansion of (2 + 1)-dimensional relativistic ideal hydrodynamic flow in heavy-ion collisions with broken longitudinal boost invariance

M. Karimabadi¹, A. F. Kord^{1,*}, and B. Azadegan

Department of Physics, Hakim Sabzevari University, P.O. Box 397, Sabzevar, Iran

 (Received 31 August 2023; accepted 9 October 2023; published 6 November 2023)

In this paper, a comprehensive analysis of the dynamical evolution of quark-gluon plasma (QGP) is presented. A perturbation approach is utilized to obtain the longitudinal and radial evolution of the fluid. The transverse fluid velocity and acceleration parameter are determined based on the influence of the generalized Bjorken model. By employing this approach, the fluid velocities, acceleration parameter, and energy density are derived. These quantities offer valuable insights into the space-time evolution of the quark-gluon plasma in heavy-ion collisions. To accurately assess these quantities, only four free parameters, namely A_1 , A_2 , q , and $\hat{\epsilon}_0$, need to be introduced, which are the only free parameters in the model. The transverse expansion of the quark-gluon plasma is characterized by two parameters, namely q and $\hat{\epsilon}_0$, which are introduced by Gubser's solution. Gubser's solutions are utilized as initial conditions at τ_0 to determine the energy density and the radial fluid velocity. Our approach, therefore, involves exploring the parameter space of these two parameters in order to find suitable values that can simulate heavy-ion collisions. It has been observed that selecting $\hat{\epsilon}_0 = 1500$ and $1/q = 6.4$ fm produces reasonable results. Furthermore, a comparison is made between the radial velocity and correction energy density obtained from our model and those obtained from the Gubser model. In addition, we ascertain the acceleration parameter of the fluid and the distribution of longitudinal energy density, which manifests as a Gaussian distribution. The expansion of the quark-gluon plasma in the longitudinal direction is distinguished by two additional parameters, denoted as A_1 and A_2 . Our methodology facilitates the derivation of equations for fluid velocities and energy densities in both the transverse and longitudinal directions of the dense and heated quark matter.

DOI: [10.1103/PhysRevD.108.094012](https://doi.org/10.1103/PhysRevD.108.094012)

I. INTRODUCTION

Based on experimental data obtained from relativistic heavy-ion collisions (HICs) conducted at RHIC and LHC, a distinct form of hot and dense nuclear matter is generated during the initial stages of collisions, commonly referred to as quark-gluon plasma (QGP). It has been observed that QGP exhibits characteristics of a strongly coupled, nearly perfect fluid. The application of relativistic hydrodynamics to describe the QGP phase has yielded promising results in heavy-ion collision experiments [1–6].

The Bjorken flow model is a straightforward scenario that characterizes the typical motion of partons following a collision [7]. This model is founded on certain assumptions, including boost invariance along the beam line, as well as translation and rotation invariance in the transverse plane. Consequently, all relevant quantities can be expressed as functions of the proper time τ in the $(\tau, x_\perp, \phi, \eta)$ Milne coordinate system. By considering the aforementioned symmetries, along with the system's invariance under reflection, one can determine the four-velocity profile,

which is given by $u^\mu = (1, 0, 0, 0)$ in the Milne coordinate system.

The Bjorken model, even in central collisions, is subject to two issues. Firstly, the model predicts that the radial flow (u_{x_\perp}) is zero due to translation invariance in the transverse plane. However, this symmetry is not realistic as the size of colliding nuclei is limited, which may result in misleading subsequent hydrodynamical flow, on which much of heavy-ions phenomenology depends. Secondly, the model predicts a flat rapidity distribution of final particles, which is inconsistent with observations at RHIC, except for a limited region around midrapidity. In realistic collisions, boost, and translation invariance are violated, and a model that is more faithful and not far from the accelerationless Bjorken picture should be investigated. Several attempts have been made to generalize the Bjorken model, such as those presented in [8–12]. Some of these attempts have included accelerating solutions of relativistic fluid dynamics to obtain more realistic estimations, as seen in [13–16]. A recent paper based on accelerating hydrodynamic description can be found in [17,18].

The objective of our research is to extend the Bjorken model in a generalized manner. Our approach assumes the

* a.f.kord@hsu.ac.ir

breaking of translation and boost invariance, while the rotational symmetry around the beam line is maintained. Our investigation focuses on central collisions, wherein we present a solution for the transverse and longitudinal expansions of a plasma, utilizing perturbation theory. We assume that the medium is formed rapidly following the collisions, with generalized Bjorken transverse and longitudinal expansions. Our aim is to derive solutions that represent the resistive relativistic hydrodynamic extension of Bjorken flow, along both the z and x_{\perp} directions.

The current study aims to examine a model that displays a partial breakdown of boost invariance in the longitudinal expansion, while simultaneously undergoing radial expansion in the transverse plane. A comprehensive analysis of the model's dynamical evolution and characteristics is provided. A novel solution of relativistic hydrodynamics in $(2 + 1)$ dimensions is derived, which is contingent upon three variables: proper time (τ), transverse coordinate (x_{\perp}), and rapidity (η). The findings of this investigation are presented, including the longitudinal and radial evolution of fluid velocities and energy density.

The present paper is structured as follows. Section II provides an exposition of the ideal relativistic hydrodynamic framework, specifically in the context of a plasma. Subsequently, we present our perturbative approach and derive analytical solutions. The findings are then discussed in Sec. III, where a comprehensive analysis of the general results is provided. The investigation focuses on the expansion of flow in both the transverse and longitudinal directions. In the transverse plane, the Gubser flow is utilized as the initial flow configuration. Subsequently, a comparison is made between the outcomes of our model and those of the Gubser flow. Furthermore, the transverse flow velocity obtained from our model is assessed in relation to the phenomenological proposition of $v_{\perp} = \frac{x_{\perp}}{50}$. Additionally, a partial breakdown of boost invariance in longitudinal expansion is demonstrated. By introducing appropriate values for the free parameters A_1 and A_2 in the solutions, satisfactory results are obtained for the rapidity fluid velocity and distribution of energy density. Finally, the last section serves to summarize the conclusions drawn from our study and highlight potential avenues for future research.

II. IDEAL RELATIVISTIC FLUID EXPANSION

In this section, we provide a succinct overview of our formalism for characterizing the assessment of QGP matter. Additionally, we take into account the rotational symmetry of the medium with respect to the beam line, which is applicable to central collisions. Consequently, we posit that all relevant quantities are dependent solely on the transverse radial coordinate x_{\perp} , the proper time τ , and the rapidity η in the Milne (τ, r, ϕ, η) coordinate system.

In this paper, we examine the scenario of an ideal nonresistive plasma consisting of massless particles. Additionally, we propose the inclusion of a thermodynamic

equation of state (EOS) that assumes the pressure to be directly proportional to the energy density, expressed as $P = 1/3\epsilon$, in order to close the set of equations. We proceed to present the energy-momentum conservation equations for an ideal fluid.

The energy-momentum conservation equations for an ideal fluid can be expressed in a covariant form, which is given by

$$d_{\mu}T^{\mu\nu} = 0, \quad (2.1)$$

where

$$T^{\mu\nu} = (\epsilon + P)u^{\mu}u^{\nu} + Pg^{\mu\nu}. \quad (2.2)$$

The energy density and pressure of the fluid are denoted by ϵ and P , respectively. In a flat spacetime, the metric tensor is represented by $g_{\mu\nu} = \text{diag}\{-, +, +, +\}$. Additionally, the four velocity of the single fluid, denoted as u^{μ} with the constraint $u_{\mu}u^{\mu} = -1$, can be expressed as $u^{\mu} = \gamma(1, \vec{v})$, where $\gamma = \frac{1}{\sqrt{1-v^2}}$.

The covariant derivative is expressed in Eq. (2.1) as follows:

$$d_{\rho}A^{\mu\nu} = \partial_{\rho}A^{\mu\nu} + \Gamma_{\rho m}^{\mu}A^{m\nu} + \Gamma_{\rho m}^{\nu}A^{\mu m}. \quad (2.3)$$

The symbols Γ_{jk}^i denote the Christoffel symbols. They are

$$\Gamma_{jk}^i = \frac{1}{2}g^{im} \left(\frac{\partial g_{mj}}{\partial x^k} + \frac{\partial g_{mk}}{\partial x^j} - \frac{\partial g_{jk}}{\partial x^m} \right). \quad (2.4)$$

One can express the conservation equations by projecting $d_{\mu}T^{\mu\nu} = 0$ along the longitudinal and transverse directions relative to u^{μ} ,

$$u_{\nu}(d_{\mu}T^{\mu\nu}_{\text{matter}} = 0) \rightarrow D\epsilon + (\epsilon + P)\Theta = 0, \quad (2.5)$$

$$\Delta_{\alpha}(d_{\mu}T^{\mu\nu}_{\text{matter}} = 0) \rightarrow (\epsilon + P)Du_{\alpha} + \nabla_{\alpha}P = 0, \quad (2.6)$$

where

$$\begin{aligned} D &= u^{\mu}d_{\mu}, & \Theta &= d_{\mu}u^{\mu}, \\ \nabla^{\mu} &= d^{\mu} + u^{\mu}D, & \Delta_{\nu}^{\alpha} &= g_{\nu}^{\alpha} + u^{\alpha}u_{\nu}. \end{aligned} \quad (2.7)$$

A. Method

In the realm of central collisions involving two nuclei, it is hypothesized that the matter undergoing expansion exhibits azimuthal symmetry. This postulation prompts the examination of the four-vector velocity of the matter, as follows:

$$\begin{aligned} u^{\mu} &= \gamma(1, v_{x_{\perp}}, 0, v_z) \\ &= (\cosh K \cosh Y, \sinh K, 0, \cosh K \sinh Y). \end{aligned} \quad (2.8)$$

The present study considers the transverse and longitudinal fluid rapidities, denoted by Y and K , respectively, with $v_z = \tanh Y$ and $v_{x_\perp} = \frac{\tanh K}{\cosh Y}$. To facilitate our analysis, we make the assumption that K is solely dependent on (x_\perp, t) , while Y is dependent on (z, t) .

The utilization of Milne coordinates is deemed more expedient in comparison to the conventional Cartesian coordinates.

$$(\tau, x_\perp, \phi, \eta) = \left(\sqrt{t^2 - z^2}, x_\perp, \phi, \frac{1}{2} \ln \frac{t+z}{t-z} \right). \quad (2.9)$$

The metric is given by

$$\begin{aligned} g^{\mu\nu} &= \text{diag}(-1, 1, 1/x_\perp^2, 1/\tau^2), \\ g_{\mu\nu} &= \text{diag}(-1, 1, x_\perp^2, \tau^2). \end{aligned} \quad (2.10)$$

By utilizing Milne coordinates, the Christoffel symbols can be readily derived. The sole nonzero symbols are as follows: $\Gamma_{\eta\eta}^\tau = \tau$, $\Gamma_{\tau\tau}^\eta = 1/\tau$, $\Gamma_{\phi\phi}^{x_\perp} = -x_\perp$, and $\Gamma_{x_\perp\phi}^\phi = 1/x_\perp$. Furthermore, in the Milne coordinate system, the four-vector velocity is expressed as follows:

$$\begin{aligned} u^\mu &= (\cosh K \cosh(Y - \eta), \sinh K, 0, \cosh K \sinh(Y - \eta)/\tau) \\ &= \bar{\gamma}(1, v_\perp, 0, 0, v_\eta/\tau), \end{aligned} \quad (2.11)$$

where $\bar{\gamma} = \cosh K(\tau, x_\perp) \cosh(Y(\tau, \eta) - \eta)$, $v_{x_\perp} = \frac{\tanh K}{\cosh(Y - \eta)}$ and $v_\eta = \tanh(Y - \eta)$.

The aforementioned assumptions facilitate the rewriting of the conservation equations in Milne coordinate. The energy and Euler equations can be expressed as follows:

$$(\epsilon + P)(v_\eta \tau \partial_\tau Y + \partial_\eta Y) + (\tau \partial_\tau \epsilon + v_\eta \partial_\eta \epsilon + \tau v_{x_\perp} \partial_{x_\perp} \epsilon) + (\epsilon + P) \left(\tau \tanh K \partial_\tau K + \frac{\tau}{\cosh(Y - \eta)} (\partial_{x_\perp} K) + \frac{\tau}{x_\perp} v_{x_\perp} \right) = 0, \quad (2.12)$$

$$(\epsilon + P) \left(\cosh K \partial_\tau K + \frac{\sinh K}{\cosh(Y - \eta)} \partial_{x_\perp} K \right) + \left(\frac{v_\eta \sinh K}{\tau} \partial_\eta P + \sinh K \partial_\tau P + \frac{\cosh K}{\cosh(Y - \eta)} \partial_{x_\perp} P \right) = 0, \quad (2.13)$$

$$\begin{aligned} (\epsilon + P)(\tau \partial_\tau Y + v_\eta \partial_\eta Y + \tau v_\eta \tanh K \partial_\tau K + \tau v_\eta v_\perp \tanh K \partial_{x_\perp} K) + \left(v_\eta \tau \partial_\tau P + v_\eta^2 \partial_\eta P + \frac{1}{\cosh K^2 \cosh^2(Y - \eta)} \partial_\eta P \right) \\ + \tau v_\eta v_{x_\perp} \partial_{x_\perp} P = 0. \end{aligned} \quad (2.14)$$

In the present study, we shall examine perturbative solutions of the aforementioned conservation equations. The desired quantities will be expressed as power series in λ_1 . The convergence of the series is not a primary concern, as it has been demonstrated that this method accurately describes the physical system under investigation. Within the framework of the perturbative approach, it is postulated that specific assumptions are made in the following manner:

$$\epsilon(\tau, x_\perp, \eta) = \epsilon^0(\tau) + \lambda_1 \epsilon^{(1)}(\tau, x_\perp, \eta) + \lambda_1^2 \epsilon^{(2)}(\tau, x_\perp, \eta) + \dots, \quad (2.15)$$

$$Y(\tau, \eta) = \eta + \lambda_1 Y^{(1)}(\tau, \eta) + \lambda_1^2 Y^{(2)}(\tau, \eta) + \dots, \quad (2.16)$$

$$K(\tau, x_\perp) = \lambda_1 k^{(1)}(\tau, x_\perp) + \lambda_1^2 K^{(2)}(\tau, x_\perp) + \dots. \quad (2.17)$$

In this context, the symbol λ_1 represents an expansion parameter that will ultimately be assigned a value of one upon completion of the calculations. To address the conservation equations under the aforementioned assumptions, it is necessary to commence by simplifying certain terms in Eqs. (2.12)–(2.14),

$$\begin{aligned} \cosh(Y - \eta) &\simeq 1 + 1/2 \lambda_1^2 Y^{(1)} + \dots, 1/\cosh(Y - \eta) \\ &\simeq 1 + \dots, v_\eta \simeq \lambda_1 Y^{(1)} + \lambda_1^2 Y^{(2)} + \dots, \\ \sinh K &\simeq \lambda_1 K^{(1)} + \lambda_1^2 K^{(2)} + \dots, \cosh K \\ &\simeq 1 + 1/2 \lambda_1^2 K^{(1)} + \dots, v_\perp \\ &\simeq \lambda_1 K^{(1)} + \lambda_1^2 K^{(2)} + \dots. \end{aligned} \quad (2.18)$$

We have retained the terms up to second order of λ_1 in our analysis. Additionally, we have taken into account that the fluid is highly relativistic, thereby rendering the rest mass contributions to the EOS negligible. Consequently, the pressure can be expressed as a simple proportionality to the energy density, i.e., $P = c_s^2 \epsilon = 1/3 \epsilon$, where $c_s = 1/3$ denotes the speed of sound. Upon substituting the aforementioned assumptions into the conservation equations (2.12)–(2.14) and identifying the powers of λ_1 , a series of equations can be obtained.

Thus, it is possible to express the equation to the first degree of λ_1 as follows:

$$\begin{aligned} \tau \partial_\tau \epsilon^{(0)} + \frac{4}{3} \epsilon^{(0)} &= 0, \\ Y^{(0)} = \eta, \quad K^{(0)} &= 0. \end{aligned} \quad (2.19)$$

The standard result for Bjorken flow, namely $\epsilon^0 = \epsilon_c(\frac{\tau_0}{\tau})^{4/3}$, has been obtained herein.

The equations resulting from the identification of terms proportional to first order in λ_1 are presented as follows:

$$\epsilon^0 Y^{(1)} + \epsilon^{(1)} + \frac{3}{4} \tau \partial_\tau \epsilon^{(1)} + \tau \epsilon^0 \partial_{x_\perp} K^{(1)} + \frac{\tau}{x_\perp} \epsilon^0 K^{(1)} = 0, \quad (2.20)$$

$$4\epsilon^0 \partial_\tau K^{(1)} + K^{(1)} \partial_\tau \epsilon^0 + \partial_{x_\perp} \epsilon^{(1)} = 0, \quad (2.21)$$

$$4\epsilon^0 \partial_\tau (\tau Y^{(1)}) + Y^{(1)} \tau \partial_\tau \epsilon^0 + \partial_\eta \epsilon^{(1)} = 0. \quad (2.22)$$

Furthermore, the equations resulting from the identification of terms that are proportional to the second order in λ_1 are expressed as follows:

$$\begin{aligned} \epsilon^2 + \frac{K^2 \epsilon^0 \tau}{x_\perp} + \frac{K^1 \epsilon^1 \tau}{x_\perp} + \epsilon^1 \tau \partial_{x_\perp} K^1 + \epsilon^0 \tau \partial_{x_\perp} K^2 + \epsilon_1 \partial_\eta Y^1 \\ + \epsilon_0 \partial_\eta Y^2 + K^1 \epsilon^0 \tau \partial_\tau K^1 + Y^1 \epsilon^0 \tau \partial_\tau Y^1 + \frac{3}{4} Y^1 \partial_\eta \epsilon^1 \\ + \frac{3}{4} K^1 \tau \partial_{x_\perp} \epsilon^1 + \frac{3}{4} \tau \partial_\tau \epsilon^2 = 0, \end{aligned} \quad (2.23)$$

$$\begin{aligned} K^2 \partial_\tau \epsilon^0 + 4K^1 \epsilon^0 \partial_{x_\perp} K^1 + 4\epsilon^1 \partial_\tau K^1 + 4\epsilon^0 \partial_\tau K^2 + \partial_{x_\perp} \epsilon_2 \\ + K^1 \partial_\tau \epsilon_1 = 0, \end{aligned} \quad (2.24)$$

$$\begin{aligned} 4\epsilon^1 Y^1 + 4\epsilon_0 Y^2 + \tau Y_2 \partial_\tau \epsilon^0 + 4\epsilon^0 Y_1 \partial_\eta Y^1 + 4\epsilon_1 \tau \partial_\tau Y^1 \\ + 4\epsilon^0 \tau \partial_\tau Y^2 + \partial_\eta \epsilon^2 + \tau Y^1 \partial_\tau \epsilon^1 = 0. \end{aligned} \quad (2.25)$$

B. First-order expansion equations

In the subsequent section, the conservation equations will be solved up to the first order expansion, as presented in Eqs. (2.20)–(2.22). The method of separation of variables will be employed to obtain the ordinary differential equations. To achieve this, we make the assumption,

$$\epsilon^{(1)}(\tau, x_\perp, \eta) = \epsilon_{x_\perp}^1(\tau, x_\perp) + \epsilon_\eta^1(\tau, \eta). \quad (2.26)$$

The aforementioned formula can be utilized to transform Eqs. (2.20)–(2.22) into simplified expressions, which are presented as follows:

$$\epsilon_{x_\perp}^{(1)} + \frac{3}{4} \tau \partial_\tau \epsilon_{x_\perp}^{(1)} + \tau \epsilon^0 \partial_{x_\perp} K^{(1)} + \frac{\tau}{x_\perp} \epsilon^0 K^{(1)} = n^2, \quad (2.27)$$

$$4\epsilon^0 \partial_\tau K^{(1)} + K^{(1)} \partial_\tau \epsilon^0 + \partial_{x_\perp} \epsilon_{x_\perp}^{(1)} = 0, \quad (2.28)$$

$$\epsilon^0 \partial_\eta Y^{(1)} + \epsilon_\eta^{(1)} + \frac{3}{4} \tau \partial_\tau \epsilon_\eta^{(1)} = -n^2, \quad (2.29)$$

$$4\epsilon^0 \partial_\tau (\tau Y^{(1)}) + Y^{(1)} \tau \partial_\tau \epsilon^0 + \partial_\eta \epsilon_\eta^{(1)} = 0. \quad (2.30)$$

The equations denoted by (2.27) and (2.28) are dependent solely upon the proper time τ and the transverse coordinate x_\perp , and serve to describe the dynamic evolution of the fluid in the transverse direction. Additionally, the equations represented by (2.29) and (2.30) are dependent solely upon the proper time τ and the space rapidity η , and serve to describe the dynamic evolution of the fluid in the longitudinal direction. It should be noted that the real number denoted by n must be identified based on physical conditions.

The amalgamation of Eqs. (2.27) and (2.28) results in a partial differential equation that solely comprises the variable of $K^{(1)}$, as given by

$$\begin{aligned} \partial_{x_\perp}^2 K^{(1)} - 3\partial_\tau^2 K^{(1)} + \frac{\partial_{x_\perp} K^{(1)}}{x_\perp} + \frac{\partial_\tau K^{(1)}}{\tau} \\ - K^{(1)} \left(\frac{1}{x_\perp^2} + \frac{1}{\tau^2} \right) = 0. \end{aligned} \quad (2.31)$$

The aforementioned partial differential equation can be solved through the method of separation of variables. The resulting general solution is as follows:

$$\begin{aligned} K^{(1)}(x_\perp, \tau) = \sum_k (c_1^k J_1(kx_\perp) + c_2^k Y_1(kx_\perp)) \\ \times \left(\tau^{2/3} \left(c_3^k J_{\frac{1}{3}}\left(\frac{k\tau}{\sqrt{3}}\right) + c_4^k Y_{\frac{1}{3}}\left(\frac{k\tau}{\sqrt{3}}\right) \right) \right). \end{aligned} \quad (2.32)$$

The Bessel functions J_1 , Y_1 , $J_{\frac{1}{3}}$, and $Y_{\frac{1}{3}}$ are of interest in this study. For each value of k , there exist four integration constants, which are typically determined by initial conditions. Alternatively, the integration constants may be reduced by imposing the initial conditions $K^{(1)}(x_\perp = 0, \tau) = 0$ and $K^{(1)}(x_\perp, \tau \rightarrow \infty) = 0$. It is important to note that, up to the first-order expansion of the energy and Euler equations, $u_\perp = \sin hK \simeq K^{(1)}$. Consequently, $c_2^k = c_4^k = 0$, yielding

$$K^{(1)}(x_\perp, \tau) = \sum_k c^k J_1(kx_\perp) \tau^{2/3} J_{\frac{1}{3}}\left(\frac{k\tau}{\sqrt{3}}\right). \quad (2.33)$$

To determine the integration constants c_k , it is necessary to have knowledge of the space-time profile of the radial velocity $u_\perp(\tau, x_\perp)$ at $\tau = \tau_0$. To achieve this, we will utilize the analytic conformal four velocity $u_\mu(\tau, x_\perp, \phi, \tau)$ discovered by Gubser [8]. The Gubser fluid velocity (u^μ) has only two nonzero components, namely u^τ and u^\perp , which describe the boost-invariant longitudinal expansion and the transverse expansion, respectively. These components are expressed as follows:

$$u^\perp(x_\perp, \tau) = \frac{qx_\perp}{\sqrt{1 + g^2(x_\perp, \tau)}}, \quad (2.34)$$

$$u^\tau(x_\perp, \tau) = \frac{1 + q^2 x_\perp^2 + q^2 \tau^2}{2q\tau\sqrt{1 + g^2(x_\perp, \tau)}}. \quad (2.35)$$

The function $g(x_\perp, \tau)$ is hereby defined as follows:

$$g(x_\perp, \tau) = \frac{1 + q^2 x_\perp^2 - q^2 \tau^2}{2q\tau}. \quad (2.36)$$

Subsequently, the conformal hydrodynamic solution shall be employed as the initial condition at τ_0 . Specifically, it is postulated that the fluid adheres to the characteristics of a Gubser fluid during the initial proper time τ_0 . Consequently, the radial fluid velocity field at τ_0 can be represented by a profile.

$$u^{(1)}(x_\perp, \tau_0) = \frac{qx_\perp}{\sqrt{1 + g^2(x_\perp, \tau_0)}}. \quad (2.37)$$

It is postulated that our proposed solution, as denoted by Eq. (2.33), is equivalent to Gubser's radial velocity solution, represented by Eq. (2.37), when evaluated at $\tau = \tau_0$.

$$\begin{aligned} u^{(1)}(x_\perp, \tau_0) &= \frac{qx_\perp}{\sqrt{1 + g^2(x_\perp, \tau_0)}} \\ &= \sum_k c^k J_1(kx_\perp) \tau_0^{2/3} J_{\frac{1}{3}}\left(\frac{k\tau_0}{\sqrt{3}}\right). \end{aligned} \quad (2.38)$$

The determination of the coefficients c^k can be achieved through the utilization of the orthogonality of Bessel functions. These coefficients are expressed as follows:

$$\begin{aligned} c^k &= \frac{2}{a^2 (J_2(\beta_{1k}))^2 J_{\frac{1}{3}}(\beta_{1k} \frac{\tau_0}{a\sqrt{3}})} \int_0^a \frac{qx_\perp^2}{\sqrt{1 + g^2(x_\perp, \tau_0)}} \\ &\quad \times J_1\left(\beta_{1k} \frac{x_\perp}{a}\right) dx. \end{aligned} \quad (2.39)$$

The k th zero of J_1 is denoted by β_{1k} . It should be noted that in the aforementioned equation, k is equivalent to the ratio of β_{1k}/a ($k = \beta_{1k}/a$). Ultimately, the transverse fluid velocity is expressed as

$$\begin{aligned} u^\perp &= u^{(1)}(x_\perp, \tau) \\ &= \sum_k \left[\frac{2}{a^2 (J_2(\beta_{1k}))^2 J_{\frac{1}{3}}(\beta_{1k} \frac{\tau_0}{a\sqrt{3}})} \right. \\ &\quad \times \left. \int_0^a \frac{qx_\perp^2}{\sqrt{1 + g^2(x_\perp, \tau_0)}} J_1\left(\beta_{1k} \frac{x_\perp}{a}\right) dx \right] \\ &\quad \times J_1(kx_\perp) \tau^{2/3} J_{\frac{1}{3}}\left(\frac{k\tau}{\sqrt{3}}\right). \end{aligned} \quad (2.40)$$

Based on our assumptions, the total energy density up to the first order in λ_1 can be given by

$$\epsilon(\tau, x_\perp, \eta) = \epsilon^0 + \epsilon_{x_\perp}^1 + \epsilon_\eta^1. \quad (2.41)$$

The density energy distribution in the transverse plane is denoted by $\epsilon_{x_\perp}^1$, while the density energy distribution in the longitudinal direction is denoted by ϵ_η^1 . To determine the transverse energy density distribution $\epsilon_{x_\perp}^1$, we combine Eqs. (2.27) and (2.28). This yields the following partial differential equation:

$$3\partial_\tau^2 \epsilon_{x_\perp}^{(1)} - \partial_{x_\perp}^2 \epsilon_{x_\perp}^{(1)} + \frac{7\partial_\tau \epsilon_{x_\perp}^{(1)}}{\tau} - \frac{\partial_{x_\perp} \epsilon_{x_\perp}^{(1)}}{x_\perp} = 0. \quad (2.42)$$

Equation (2.42) may be solved through the method of separation of variables. The general solution that is as follows:

$$\begin{aligned} \epsilon_{x_\perp}^{(1)}(x_\perp, \tau) &= \sum_k (c_1^k J_0(kx_\perp) + c_2^k Y_0(kx_\perp)) \\ &\quad \times \left(\tau^{-2/3} \left(c_3^k J_{\frac{2}{3}}\left(\frac{k\tau}{\sqrt{3}}\right) + c_4^k Y_{\frac{2}{3}}\left(\frac{k\tau}{\sqrt{3}}\right) \right) \right). \end{aligned} \quad (2.43)$$

To ensure consistency between the above solution and the transverse fluid velocity equation (2.40), it is necessary to set $c_{2,4}^k = 0$. Consequently, the solution can be expressed as follows:

$$\epsilon_{x_\perp}^{(1)}(x_\perp, \tau) = \sum_k c'^k J_0(kx_\perp) \tau^{-2/3} J_{\frac{2}{3}}\left(\frac{k\tau}{\sqrt{3}}\right). \quad (2.44)$$

Furthermore, it is posited that the fluid being studied exhibits characteristics akin to those of Gubser's inviscid hydrodynamic fluid at the specific time of $\tau = \tau_0$. As a result, the value of $\epsilon_{x_\perp}^{(1)}(x_\perp, \tau_0)$ can be expressed as

$$\epsilon_{x_\perp}^{(1)}(x_\perp, \tau_0) = \epsilon_g(x_\perp, \tau_0) - \epsilon_0(\tau_0), \quad (2.45)$$

where $\epsilon_g(x_\perp, \tau)$ is given by [8]

$$\epsilon_g(x_\perp, \tau) = \frac{\hat{\epsilon}_0}{\tau^{4/3}} \frac{(2q)^{8/3}}{[1 + 2q^2(\tau^2 + x_\perp^2) + q^4(\tau^2 - x_\perp^2)^2]^{4/3}}. \quad (2.46)$$

Gubser's energy density for a conformal inviscid fluid is denoted by ϵ_g while $\hat{\epsilon}$ and q are two constants. The reciprocal of q is directly proportional to the transverse size of the plasma. By utilizing Eqs. (2.44)–(2.46), and the orthogonality of Bessel functions, one can derive the coefficients in (2.44). These coefficients are

$$c^{lk} = \frac{2}{a^2 (J_1(\beta_{0k}))^2 J_{\frac{2}{3}}(\beta_{0k} \frac{\tau_0}{a\sqrt{3}})} \int_0^a x_{\perp} (\epsilon_g(x_{\perp}, \tau_0) - \epsilon_0(\tau_0)) \times J_0\left(\beta_{0k} \frac{x_{\perp}}{a}\right) dx_{\perp} \quad (2.47)$$

with β_{0k} being the k th zero of J_0 , where $k = \beta_{0k}/a$. The k th zero of the Bessel function of the first kind, denoted as J_0 , is represented by β_{0k} . It is noteworthy that in the aforementioned equation, the value of k is equivalent to the ratio of β_{0k}/a . Ultimately, the distribution of transverse energy density is expressed as follows:

$$\epsilon_{x_{\perp}}^{(1)}(x_{\perp}, \tau) = \sum_k \left[\frac{2}{a^2 (J_1(\beta_{0k}))^2 J_{\frac{2}{3}}(\beta_{0k} \frac{\tau_0}{a\sqrt{3}})} \int_0^a x_{\perp} (\epsilon_g(x_{\perp}, \tau_0) - \epsilon_0(\tau_0)) J_0\left(\beta_{1k} \frac{x_{\perp}}{a}\right) dx_{\perp} \right] \times J_0(kx_{\perp}) \tau^{-2/3} J_{\frac{2}{3}}\left(\frac{k\tau}{\sqrt{3}}\right). \quad (2.48)$$

C. Longitudinal expansion

In this section, we shall examine the evolution of longitudinal expansion in an ideal fluid. The Bjorken model represents the most elementary approach to characterizing the longitudinal expansion of a fluid [7]. The Bjorken model depicts a flow that remains invariant under a Lorentz boost along the longitudinal direction. However, in reality, the longitudinal expansion may be influenced by acceleration, and nonboost invariant initial conditions may exist, leading to the absence of a rapidity plateau [14–16]. Further references and information can be found in [17–20].

The present study investigates a model that exhibits partial breakdown of boost invariance in the longitudinal expansion. The approach taken involves the utilization of power series expansions up to the first order in λ_1 , leading to the following assumption:

$$Y^{(1)}(\tau, \eta) = Y(\tau, \eta) - \eta. \quad (2.49)$$

$Y^{(1)}$ denotes the acceleration of the fluid in the longitudinal direction. By combining Eqs. (2.29) and (2.30), a partial

differential equation for $Y^{(1)}$ can be derived, which is expressed as follows:

$$\partial_{\eta}^2 Y^{(1)} - 3\tau^2 \partial_{\tau}^2 Y^{(1)} - 5\tau \partial_{\tau} Y^{(1)} = 0. \quad (2.50)$$

The equation can be solved through the method of separation of variables. The general solution is given by

$$Y^{(1)}(\tau, \eta) = \frac{A_0}{\tau^{2/3}} + \sum_{m=1} A_m \tau^{-\frac{1}{3} - \frac{1}{3}\sqrt{3 + \frac{1}{m^2}}} \times [\sin h(m\eta) + B_m \cos h(m\eta)]. \quad (2.51)$$

In the context, the constant coefficients A_0 , A_m , and B_m can be determined upon the physical conditions. Assuming that the limit of $Y(\tau, \eta \rightarrow 0) \rightarrow \eta$, it can be deduced that both A_0 and B_m must be equivalent to zero. As a result, the formula for the correction fluid rapidity $Y^1(\tau, \eta)$ can be derived,

$$Y^{(1)}(\tau, \eta) = \sum_{m=1} A_m \tau^{-\frac{1}{3} - \frac{1}{3}\sqrt{3 + \frac{1}{m^2}}} [\sin h(m\eta)]. \quad (2.52)$$

To ascertain the coefficients A_m , it is necessary to possess knowledge of the flow rapidity profile $Y(\tau = \tau_0, \eta) = \eta + Y^1(\tau_0, \eta)$. However, for the sake of simplicity, we limit ourselves to retaining solely the first two terms in Eq. (2.52). Consequently, the corrected flow rapidity can be expressed as

$$Y^{(1)}(\tau, \eta) = \frac{A_1}{\tau} \sin h(\eta) + A_2 \tau^{-\frac{1}{3}(1+\sqrt{13})} \sin h(2\eta). \quad (2.53)$$

Furthermore, in order to determine the correction for energy density distribution in the longitudinal direction ϵ_{η}^1 , it is feasible to integrate Eqs. (2.29) and (2.30). As a result, the partial differential equation for ϵ_{η}^1 can be formulated as follows:

$$\partial_{\eta}^3 \epsilon_{\eta}^{(1)} - 3\tau^2 \partial_{\tau}^2 \partial_{\eta} \epsilon_{\eta}^{(1)} - 13\tau \partial_{\tau} \partial_{\eta} \epsilon_{\eta}^{(1)} - 8\partial_{\eta} \epsilon_{\eta}^{(1)}. \quad (2.54)$$

The aforementioned equation can be solved through the process of separating variables. The general solution is given by

$$\begin{aligned} \epsilon_{\eta}^{(1)}(\tau, \eta) = & (A_0^1 + A_0^2 \eta + A_0^3 \eta^2) \left(\frac{A_0^1}{\tau^2} + \frac{A_0^2}{\tau^{4/3}} \right) + (B_1^1 \cos h(\eta) + B_1^2 \sin h(\eta) + B_1^3) \left(\frac{B_1^1}{\tau^{7/3}} + \frac{B_1^2}{\tau} \right) \\ & + (C_2^1 \cos h(2\eta) + C_2^2 \sin h(2\eta) + C_2^3) (C_2^1 \tau^{-\frac{5}{3} - \frac{\sqrt{13}}{3}} + C_2^2 \tau^{-\frac{5}{3} + \frac{\sqrt{13}}{3}}) \\ & + \sum_{m=3} (D_m^1 \tau^{-\frac{5}{3} - \frac{1}{3}\sqrt{3 + \frac{1}{m^2}}} (\cos h(m\eta) - D_m^1 \sin h(m\eta) + D_m^2). \end{aligned} \quad (2.55)$$

The determination of constant coefficients can be accomplished by means of physical conditions. Furthermore, by substituting both solutions, as given in Eqs. (2.52) and (2.55), into Eq. (2.30), one obtains

$$\begin{aligned}
\epsilon_{\eta}^{(1)}(\tau, \eta) &= (B_1^1 \cos h(\eta)) \left(\frac{B_1^1}{\tau^{7/3}} + \frac{B_1^2}{\tau} \right) \\
&+ (C_2^1 \cos h(2\eta)) (C_2^1 \tau^{-\frac{5}{3} - \frac{\sqrt{13}}{3}} + C_2^2 \tau^{-\frac{5}{3} + \frac{\sqrt{13}}{3}}) \\
&+ \sum_{m=3} (D_m^1 \tau^{-\frac{5}{3} - \frac{1}{m}} \sqrt{3 + \frac{1}{m^2}}) (\cos h(m\eta)). \quad (2.56)
\end{aligned}$$

Upon consideration of the particular solution represented by Eq. (2.53) pertaining to the fluid rapidity, the solution for the correction energy density ϵ_{η}^1 can be expressed as follows:

$$\begin{aligned}
\epsilon_{\eta}^{(1)}(\tau, \eta) &= \frac{4}{3} \epsilon_c \tau_0^{4/3} A_1 \frac{\cos h(\eta)}{\tau^{7/3}} \\
&+ \frac{2}{3} (\sqrt{13} - 1) \epsilon_c \tau_0^{4/3} A_2 \tau^{-\frac{5}{3} - \frac{\sqrt{13}}{3}} \cos h(2\eta). \quad (2.57)
\end{aligned}$$

The above equation comprises of two distinct terms that delineate the energy density distribution in the longitudinal expansion. The following section will elucidate the behavior of these physical quantities.

In this section, a perturbation expansion has been employed to analyze the conservation equations mentioned earlier. By identifying terms that are proportional to the second order in λ_1 , the resulting equations have been obtained. However, the conservation equations have only been solved up to the first-order expansion. The general solutions obtained are consistent with the findings presented in Ref. [12]. The authors of Ref. [12] have investigated a small perturbation added to the Bjorken flow, represented as $P = P_0 + P_1$ (the pressure field) and $u^\mu = u_0^\mu + u_1^\mu$ (the fluid velocity field). They have derived the linearized hydrodynamic equations and subsequently solved them to determine the general solutions. It is worth noting that their linearized hydrodynamic equations and general solutions align with our solutions up to the first-order expansion. However, the physical solutions have not been obtained. To obtain the physical solutions, knowledge of the flow profile at the initial proper time τ_0 is required. By utilizing the proper initial conditions, the coefficients of the general solutions can be determined. In our case, the physical solutions in transverse expansions have been obtained by utilizing the analytic conformal solutions [8] at $\tau = \tau_0$, and the orthogonality of Bessel functions. In the longitudinal expansions, the constant coefficients A_0 , A_m , and B_m have been determined based on physical conditions and some simplifications. Finally, the energy density, transverse flow velocity, and flow rapidity have been derived.

III. RESULTS AND DISCUSSIONS

In this section, we provide a comprehensive analysis of the dynamical evolution and characteristics of our model, utilizing a perturbation approach. Our investigation focuses

on the longitudinal and radial evolution of the fluid, which is reflected in the transverse fluid velocity and acceleration parameter, respectively, due to the influence of the generalized Bjorken model. Through our perturbation approach, we derive the corrected fluid velocities, acceleration parameter, and energy density. These quantities provide valuable insights into the space-time evolution of the quark-gluon plasma in heavy-ion collisions.

The aforementioned quantities are crucial in comprehending the space-time evolution of the quark-gluon plasma in heavy-ion collisions. To accurately assess these quantities, it is imperative to establish the values of the constants A_1 , A_2 , q , and $\hat{\epsilon}_0$. These are the only free parameters in our model.

The initial conditions for the transverse expansion of the quark-gluon plasma are characterized by two parameters, namely q and $\hat{\epsilon}_0$, which are introduced by Gubser's solution. Together, they determine the initial energy density profile of the plasma at some early time that should be comparable to or greater than the time at which a hydrodynamic description becomes valid. The parameter q also implicitly determines the radial velocity profile at early time of the hydrodynamic evolution. Our approach, therefore, is to explore the two parameter space looking for reasonable values to mock up heavy-ion collisions. We have found that choosing $\hat{\epsilon}_0 = 1500$ and $1/q = 6.4$ fm yields reasonable results, as we shall show below.

In order to accurately depict the space-time assessment of longitudinal expansion of QGP, it is imperative to establish fixed parameters, namely A_1 and A_2 , that align with phenomenological analyses. Regrettably, in this particular study, the aforementioned parameters have been selected based on the following condition:

$$\begin{aligned}
\frac{\epsilon_{\eta}^{(1)}(\tau, \eta)}{\epsilon_0(\tau)} &< \frac{\epsilon_{\eta}^{(1)}(\tau_0, \eta = 0)}{\epsilon_0(\tau_0)} \\
&= \frac{4}{3} A_1 \frac{1}{\tau_0} + \frac{2}{3} (\sqrt{13} - 1) A_2 \tau_0^{-\frac{1}{3} - \frac{\sqrt{13}}{3}} \ll 1. \quad (3.1)
\end{aligned}$$

For our numerical computation, we have opted to utilize the values of $A_1 = 0.3$ and $A_2 = -0.07$.

A. Transverse expansion

This subsection presents the numerical results of the transverse velocity and energy density obtained through our perturbation approach. These two quantities aid in comprehending the transverse evolution of the quark-gluon plasma in heavy-ion collisions. Through our analysis, the value of ϵ_0 has been determined to be $5.4 \text{ GeV}/\text{fm}^3$ at a proper time of approximately $\tau = 1 \text{ fm}$, as reported in Ref. [21]. The parameters $\hat{\epsilon}_0 = 1500$ and $1/q = 6.4 \text{ fm}$ have been chosen for our study. Subsequently, we display the transverse fluid velocity ($v_{\perp} = \frac{u_{\perp}}{u_{\tau}}$) and the transverse energy density distribution [$e_{\perp}^1(\tau, x_{\perp})$].

Figure 1 illustrates the transverse velocity, denoted as v_{\perp} , which is defined as the ratio of the transverse component of the four-velocity, u^{\perp} , to its temporal component, u^{τ} . The plot depicts v_{\perp} as a function of x_{\perp} or τ , while either τ or x_{\perp} is held constant. Additionally, a comparison with Gubser's transverse velocity is presented. The transverse velocity's dependence on x_{\perp} exhibits a comparable shape to that of Gubser's work. Nevertheless, the transverse velocity's dependence as a function of τ , as depicted in the right panel of Fig. 1, deviates from the Gubser flow for $\tau > 5 fm$. This suggests that our flow exhibits a longer life time compared to the Gubser flow. Figure 2 displays the transverse velocity v_{\perp} as a function of either x_{\perp} for various values of x_{\perp} or τ , respectively. Notably, it is observed that v_{\perp} increases for larger values of τ (at a fixed x_{\perp}) or for larger values of x_{\perp} (at a fixed τ). This phenomenon is a consequence of the assumption of conformal symmetry in the initial conditions, which impacts the spatiotemporal evolution of the transverse expansion of the fluid [8]. Nevertheless, the energy density experiences a significant

decrease and ultimately reaches zero at a large value of x_{\perp} , as depicted in the right panel of Fig. 5. This peculiar phenomenon is attributed to a complete failure of the derivative expansion, which serves as the foundation of hydrodynamics. To elucidate this aspect, we present the two-dimensional fluid velocity and the contours of constant temperature in Fig. 3. The plot has been exhibited for values of (τ, x_{\perp}) wherein ϵ is positive. The prominently delineated red contour corresponds to the temperature of 130 MeV. It is suggested that the region of flow in which the temperature exceeds 130 MeV may be considered as the quark-gluon plasma. It is important to note that the temperature of 130 MeV is approximately the decoupling temperature in a Cooper-Frye treatment. Beyond this temperature, the genuine degrees of freedom are those of a nearly free hadron gas, rather than a fluid. The hydrodynamic approximation is deemed invalid when the temperature falls below 130 MeV. In summary, our hydrodynamic model approximation is applicable only for values of x_{\perp} and τ where the temperature exceeds 130 MeV. A comparison with the findings of

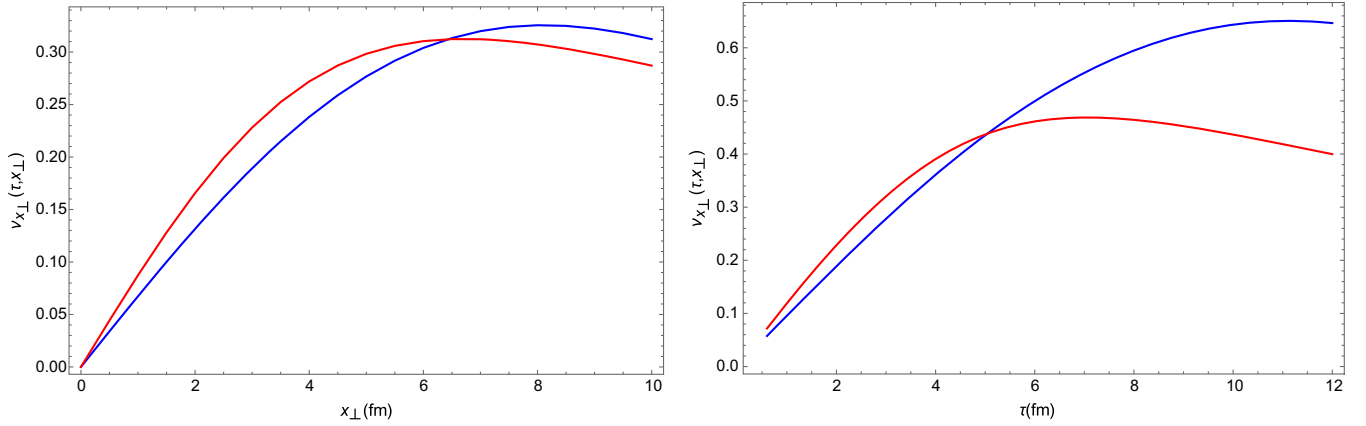


FIG. 1. Left: the transverse velocity $v_{\perp} = \frac{u^{\perp}}{u^{\tau}} \simeq K^1(\tau, x_{\perp})$ in terms of x_{\perp} for $\tau = 2$. Right: the transverse velocity in terms of τ for $x_{\perp} = 3$. The blue curve correspond to present work and the red curve correspond to [8]. It is measured in fm/c, with $q = 1/6.4 \text{ fm}^{-1}$.

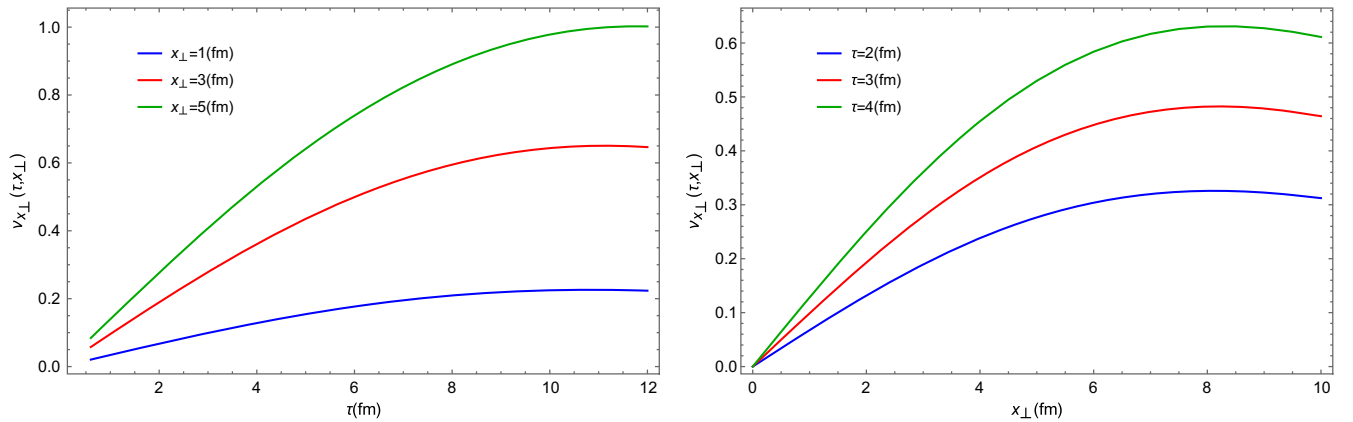


FIG. 2. Left: the transverse velocity v_{\perp} as a function of proper time τ for several values of transverse radius x_{\perp} . Right: the transverse velocity v_{\perp} as a function of transverse radius x_{\perp} for several values of proper time τ . It is measured in fm/c, with $q = 1/6.4 \text{ fm}^{-1}$.

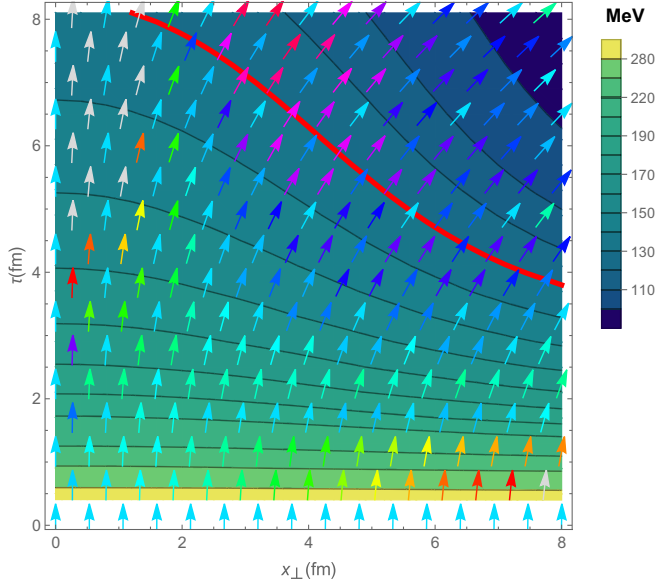


FIG. 3. The two-dimensional fluid velocity ($u^r/\sqrt{u_r^2 + u_\perp^2}$, $u^\perp/\sqrt{u_r^2 + u_\perp^2}$) is plotted with parameters chosen as $q = 1/6.4 \text{ fm}^{-1}$, $\tau_0 = 1 \text{ fm}$, $\hat{e}_0 = 1500$, and $e_c = 5.4 \text{ GeV}/\text{fm}^3$.

Ref. [8] suggests that a slightly larger value of τ and a smaller value of x_\perp would be more appropriate in our case. This indicates that the spatial regain of the QGP is smaller compared to the Gubser flow, but the lifetime of the system in the plasma phase is longer than in the Gubser case.

Figure 4 displays the energy density $\epsilon(\tau, x_\perp) = \epsilon_0(\tau) + \epsilon_{x_\perp}^1(\tau, x_\perp)$ as a function of x_\perp or τ at a fixed value of either τ or x_\perp . It is important to note that the total energy density is given by $\epsilon(\tau, x_\perp, \eta) = \epsilon_0 + \epsilon_{x_\perp}^1 + \epsilon_\eta^1$. The analysis also includes a comparison with the Gubser flow. The results indicate that the majority of energy distribution is concentrated at small values of $x_\perp < 5 \text{ fm}$. Furthermore, the left panel of Fig. 4 demonstrates that the spatial distribution

of energy density is comparatively smoother than that of the Qubser flow's energy density. Figure 5 shows the energy density $\epsilon(\tau, x_\perp)/\epsilon_0$ as a function of x_\perp for different values of τ or as a function of τ for different values of x_\perp , respectively.

To evaluate the efficacy of our model, we derive the coefficients c^k in (2.33) by employing an alternative radial flow profile, as investigated in [22], at the initial proper time τ_0 . The coefficients c^k are obtained through the utilization of the orthogonality of Bessel functions, and are expressed as follows:

$$c^k = \frac{2}{a^2 (J_2(\beta_{1k}))^2 J_{\frac{1}{3}}(\beta_{1k} \frac{\tau_0}{a\sqrt{3}})} \times \int_0^a \frac{\tan h(x_\perp/50)}{\bar{\gamma}} J_1\left(\beta_{1k} \frac{x_\perp}{a}\right) dx. \quad (3.2)$$

Upon conducting a first order expansion calculation, it has been determined that $\bar{\gamma} \simeq 1$. As a result, the transverse fluid velocity can be expressed as

$$v^\perp \simeq u^{(1)}(x_\perp, \tau) = \sum_k \left[\frac{2}{a^2 (J_2(\beta_{1k}))^2 J_{\frac{1}{3}}(\beta_{1k} \frac{\tau_0}{a\sqrt{3}})} \times \int_0^a \tan h(x_\perp/50) J_1\left(\beta_{1k} \frac{x_\perp}{a}\right) dx_\perp \right] \times J_1(kx_\perp) \tau^{2/3} J_{\frac{1}{3}}\left(\frac{k\tau}{\sqrt{3}}\right). \quad (3.3)$$

Figure 6 displays the transverse velocity $v_\perp \simeq u^1$ as a function of transverse radius x_\perp for various values of the proper time τ . The radial flows are compared, with the coefficients c^k being derived from distinct initial conditions. The transverse velocity was displayed by the solid

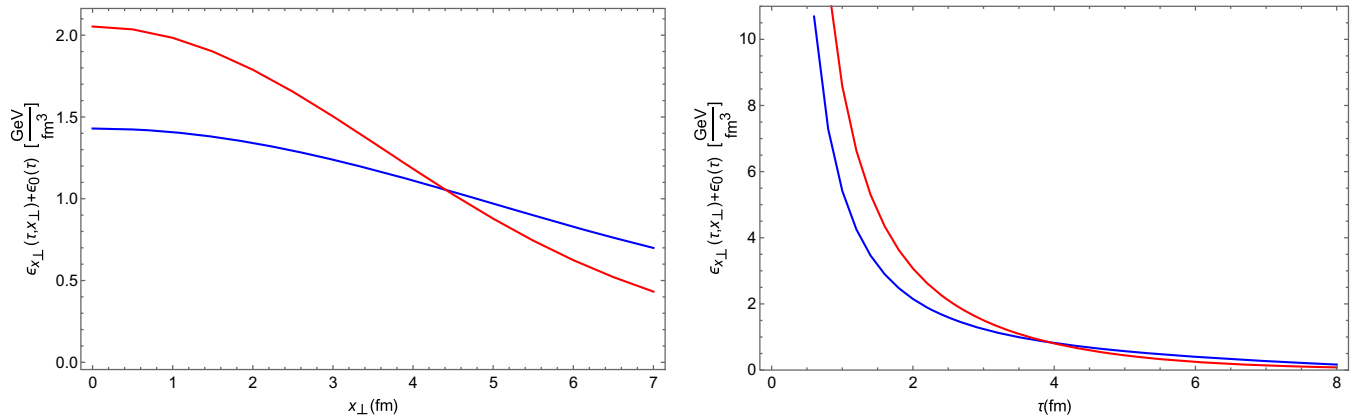


FIG. 4. Left: the total energy density $\epsilon(\tau, x_\perp)$ as a function of transverse radius x_\perp at $\tau = 3 \text{ fm}$. Right: the total energy density $\epsilon(\tau, x_\perp)$ as a function of proper time τ at $x_\perp = 3 \text{ fm}$. The blue curve correspond to present work and the red curve to [8]. With parameters chosen as $q = 1/6.4 \text{ fm}^{-1}$, $\tau_0 = 1 \text{ fm}$, $\hat{e}_0 = 1500$, and $e_c = 5.4 \text{ GeV}/\text{fm}^3$.

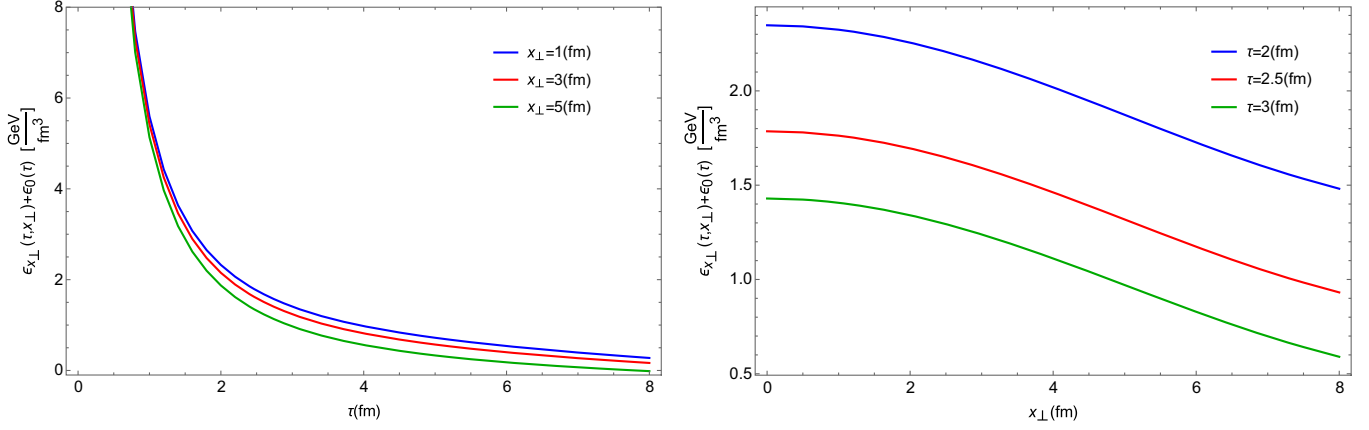


FIG. 5. Left: $\epsilon(\tau, x_{\perp})$ in terms of proper time τ for different value of x_{\perp} . Right: $\epsilon(\tau, x_{\perp})$ in terms of transverse radius x_{\perp} for different value of τ . With parameters chosen as $q = 1/6.4 \text{ fm}^{-1}$, $\tau_0 = 1 \text{ fm}$, $\hat{\epsilon}_0 = 1500$, and $\epsilon_c = 5.4 \text{ GeV/fm}^3$.

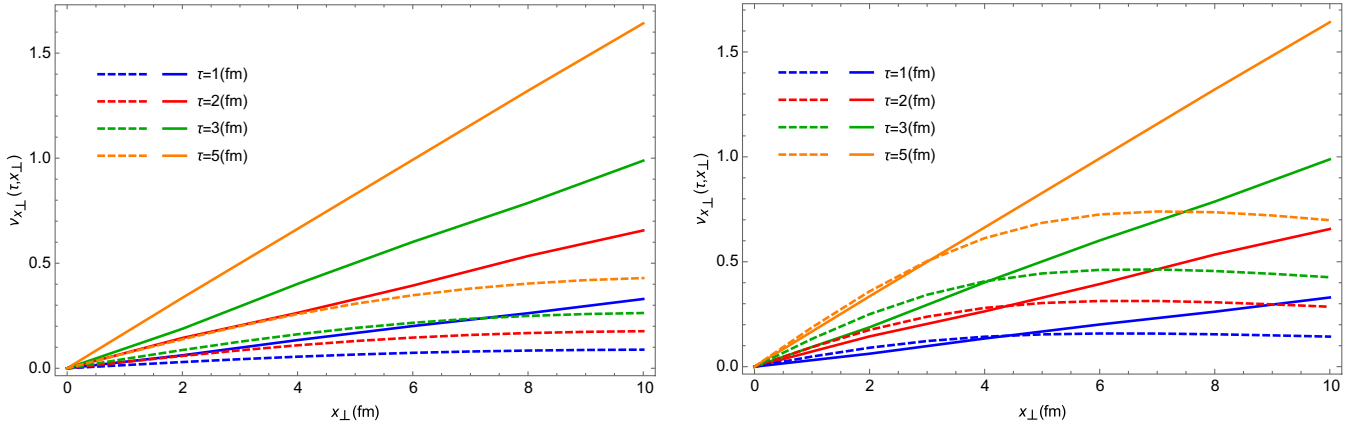


FIG. 6. The transverse velocity v_{\perp} as a function of transverse radius x_{\perp} for several values of τ , measured in fm. The solid lines displayed the transverse velocities where c^k are obtained from the phenomenological proposal $v_{\perp} = \tan h x_{\perp}/50$ at $\tau_0 = 0.6 \text{ fm}$. The dashed lines displayed the transverse velocities where c^k are obtained from the Gubser proposal at $\tau_0 = 0.6 \text{ fm}$. The initial proper time is chosen as $\tau_0 = 0.6 \text{ fm}$. Two different values of $q = 1/11.24266 \text{ fm}^{-1}$ (left panel) and $q = 1/6.4 \text{ fm}^{-1}$ (right panel) are chosen for the Gubser proposal as initial conditions.

lines utilizing the initial conditions derived from the phenomenological proposal $v_{\perp} = \tan h \frac{x_{\perp}}{50}$ at $\tau_0 = 0.6$. The transverse velocity, derived from the initial conditions proposed by Gubser at $\tau_0 = 0.6$ for two distinct values of q , was represented by dashed lines in the plot. The results of our study suggest that, for a value of q equal to $1/6.4 \text{ fm}^{-1}$ and $x_{\perp} < 5$, the radial velocity of systems with varying initial conditions converge to a common late-time behavior. However, it is observed that this convergence does not occur when q deviates from the aforementioned value, as depicted in the left panel of Fig. 6. This finding is in accordance with the results presented in [23], which have also concluded that selecting $q = 1/6.4 \text{ fm}$ produces reasonable spectra for both pions and protons.

When comparing with phenomenological studies, it is important to note that the linear solution is only applicable for small perturbations. Therefore, the reliability of our

results may be limited to the qualitative level. However, our linear solution may have relevance to certain aspects of the expanding fluid in heavy-ion collisions. Additionally, it should be emphasized that this work presents an approximate calculation, which can be valuable for cross-checking current and future numerical calculations in specific limiting regions. It is worth noting that a comprehensive description of the dynamical evolution of the created fireball can be effectively achieved through the use of relativistic hydrodynamics, including viscous corrections. To accomplish this, a numerical code that solves the equations of $(1 + 3)$ -dimensional relativistic hydrodynamics is required.

B. The longitudinal expansion

The QGP system that undergoes evolution in relativistic heavy-ion collisions is inherently nonboost invariant.

The hot medium is confined within a finite range of rapidity, while the system remains dilute outside of this window. Within this subsection, we present a novel set of solutions to the hydrodynamic equations that do not exhibit boost invariance. We illustrate the impact of a disrupted longitudinal boost invariant motion on the solutions of relativistic hydrodynamics. Our general solutions, denoted as (2.52) and (2.56), delineate the effects of nonboost longitudinal expansion of the fluid. These solutions have been employed to approximate the correction fluid rapidity $v_\eta(\tau, \eta) \simeq Y^1(\tau, \eta)$ and the correction longitudinal energy density ϵ_η^1 that arise from the hydrodynamic solutions expressed in Eqs. (2.53) and (2.57).

In this study, we have conducted an investigation into the dynamical evolution of the fluid rapidity. The results of this investigation are presented in Fig. 7, which depicts the evolution of $\lambda = \frac{Y}{\eta} = \frac{Y^1(\tau, \eta) + \eta}{\eta}$ as a function of η for various values of τ (the left panel), or as a function of τ for different values of η (the right panel). It is important to note that λ is commonly referred to as the acceleration parameter [19], as

it characterizes the acceleration of the longitudinal flow. The analysis reveals that the acceleration parameter exhibits a decreasing trend as the absolute value of η increases. However, it is noteworthy that a plateau is observed for the late-time regime. The plotted data indicates that an increase in η leads to a reduction in the acceleration parameter, and over time, the attenuation of $\lambda(\tau, \eta)$ occurs over a broad range of rapidity. This implies that the flow experiences a greater acceleration at lower values of η or τ .

Figure 8 shows the ratio of energy density $\epsilon(\tau, \eta)/\epsilon_0$ in terms of η for several values of τ (left panel), or in terms of τ for several values of η (right panel). In accordance with the left panel of Fig. 8, the energy density rapidity distribution at the early time when QGP is formed has a Gaussian shape, while at the late time it becomes rather a plateau. It is found that energy density slowly flows toward high rapidity at the later time. The ratio of energy density $\epsilon(\tau, \eta)/\epsilon_0$ in terms of η (the left panel) or in terms of proper time τ (right panel) is exhibited in Fig. 9 for several different values of A_1 and A_2 . As is evident, the shape of energy density profile depends

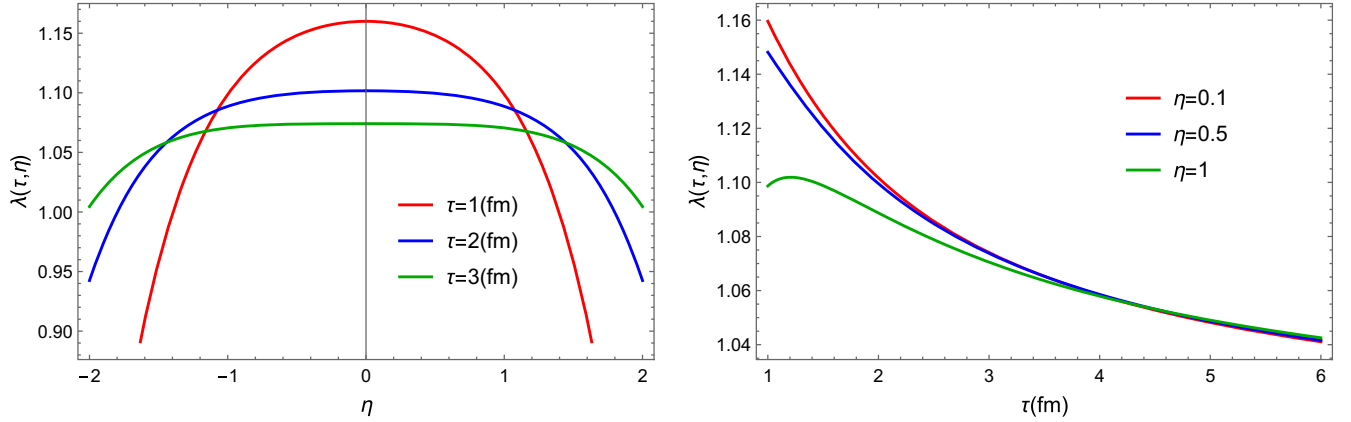


FIG. 7. Right: acceleration parameter $\lambda(\tau, \eta) = Y(\tau, \eta)/\eta \simeq \frac{Y^1(\tau, \eta) + \eta}{\eta}$ in terms of η with different value of τ . Right: $\lambda(\tau, \eta)$ in terms of τ with different value of η . The values $A_1 = 0.3$ and $A_2 = -0.07$ are chosen.

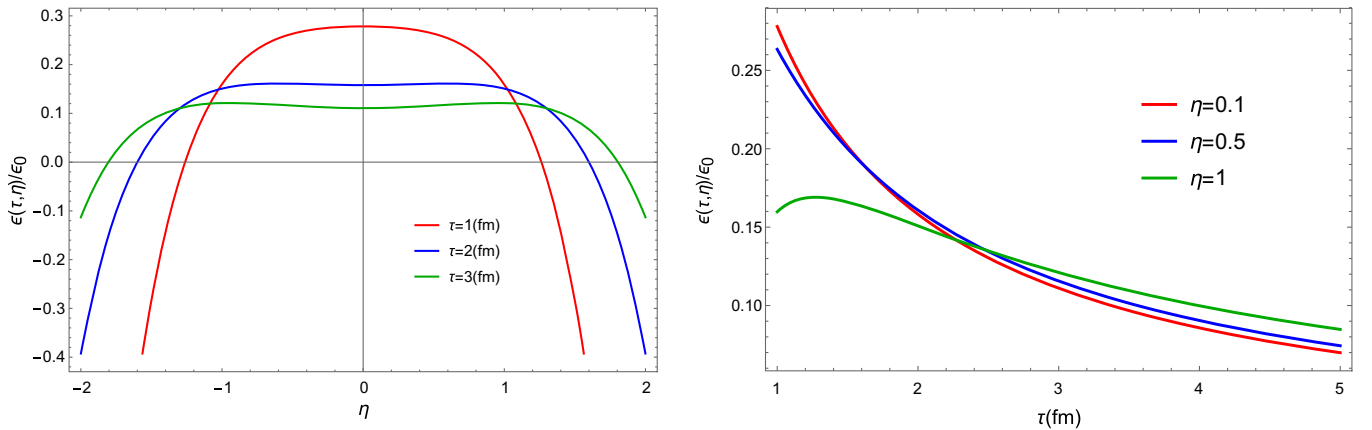


FIG. 8. Right: $\epsilon_\eta(\tau, \eta)/\epsilon_0$ as a function of the space-time rapidity η with different values of τ . Right: $\epsilon_\eta(\tau, \eta)/\epsilon_0$ as a function of proper time τ with different value of η . The values $A_1 = 0.3$ and $A_2 = -0.07$ are chosen.

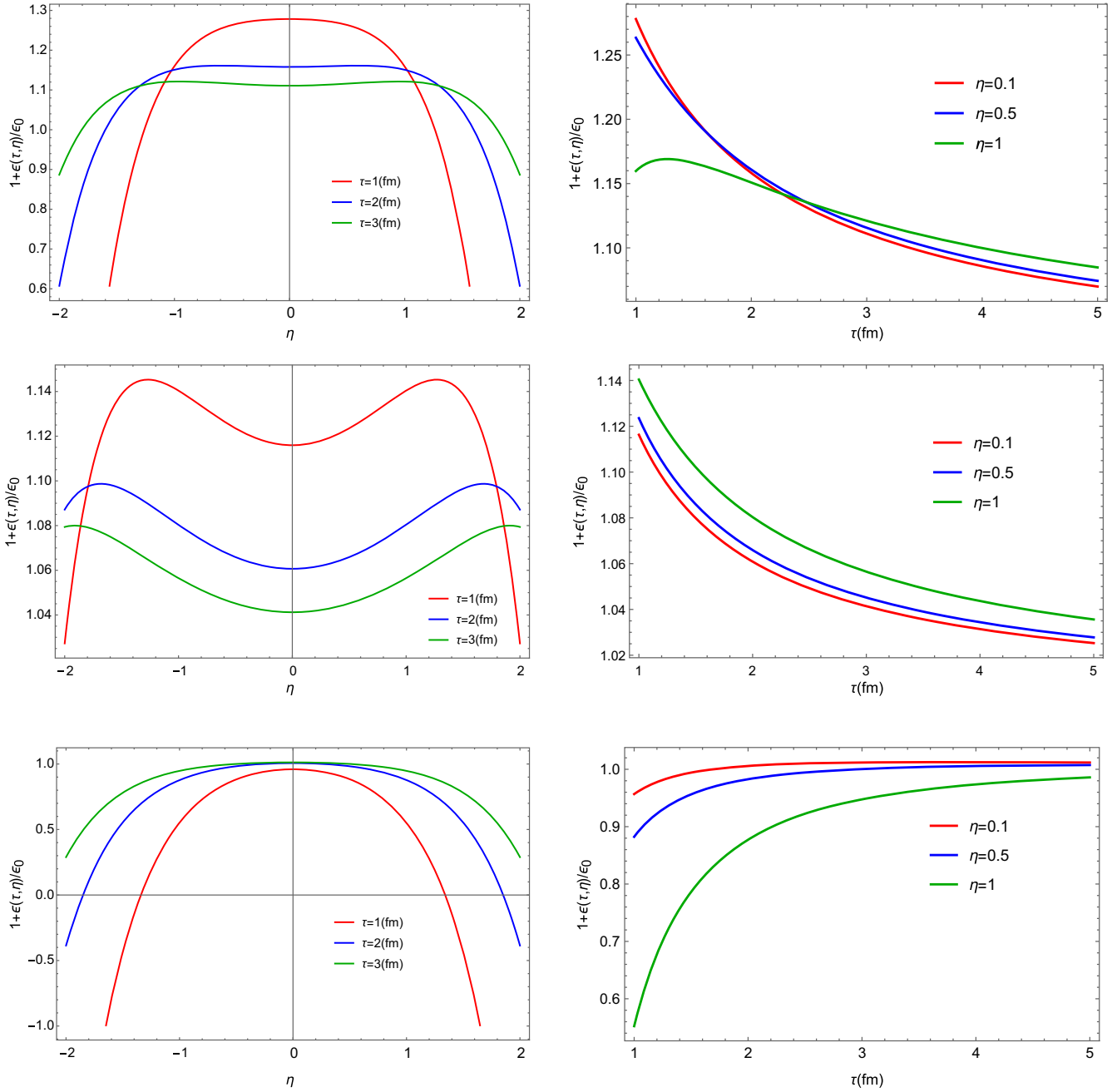


FIG. 9. Left: $(\epsilon_\eta(\tau, \eta) + \epsilon_0)/\epsilon_0$ as a function of the space-time rapidity η with different values of τ . Right: $(\epsilon_\eta(\tau, \eta) + \epsilon_0)/\epsilon_0$ as a function of proper time τ with different values of η . The values A_1, A_2 are chosen: $A_1 = 0.3, A_2 = -0.07$ (top panel), $A_1 = 0.1, A_2 = -0.01$ (middle), and $A_1 = 0.1, A_2 = -0.1$ (bottom) respectively.

on the free parameters A_1, A_2 . These parameters should be fixed with the rapidity dependence of particle yield, which can be computed in the theory and measured in experiments. Also, in left panel of Fig. 9, we demonstrate $\epsilon(\tau, \eta)/\epsilon_0$ in terms of rapidity for different fixed proper times. It can be seen that at the early times, the plot has a Gaussian distribution, while at the late time, it becomes a plateau around the small rapidity.

Finally, Fig. 10 illustrates the total energy density $\epsilon(\tau, x_\perp, \eta)$ as a function of x_\perp and η at a fixed value of $\tau = 2$ fm, or as a function of τ and η at a fixed value of $x_\perp = 3$ fm. The figure indicates that the energy density is most significantly altered in the central region, where a reduction is observed in both cases. Additionally, Fig. 11 displays the total energy density $\epsilon(\tau, x_\perp, \eta)$ as a function of τ and x_\perp at a fixed value of $\eta = 2$.

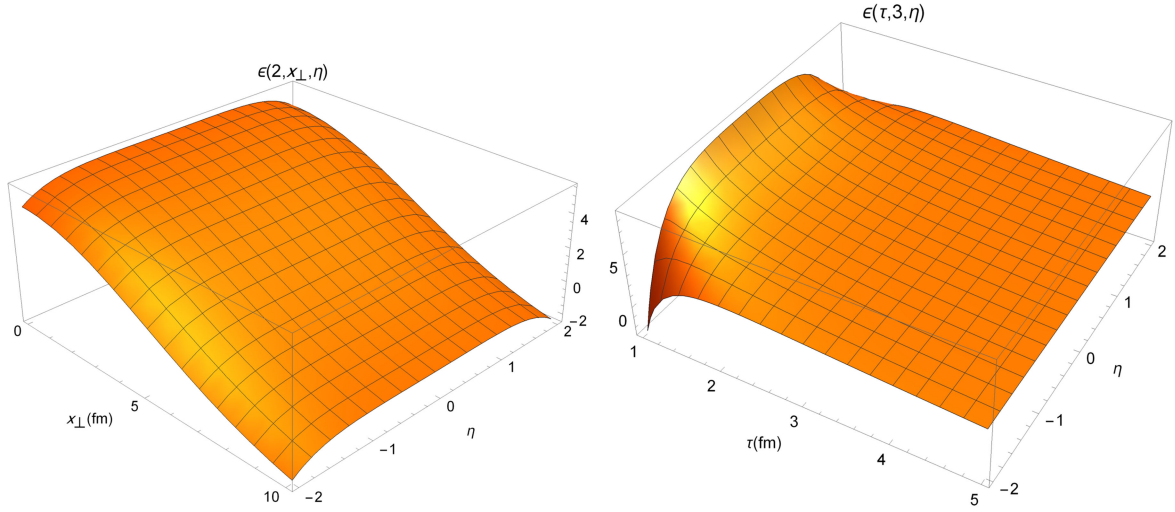


FIG. 10. $\epsilon(\tau, x_{\perp}, \eta)$. The values $A_1 = 0.3$, $A_2 = -0.07$, $q = 1/6.4 \text{ fm}^{-1}$, $\tau_0 = 1 \text{ fm}$, $\epsilon_c = 5.4$, and $\hat{\epsilon}_0 = 1500$ are chosen.

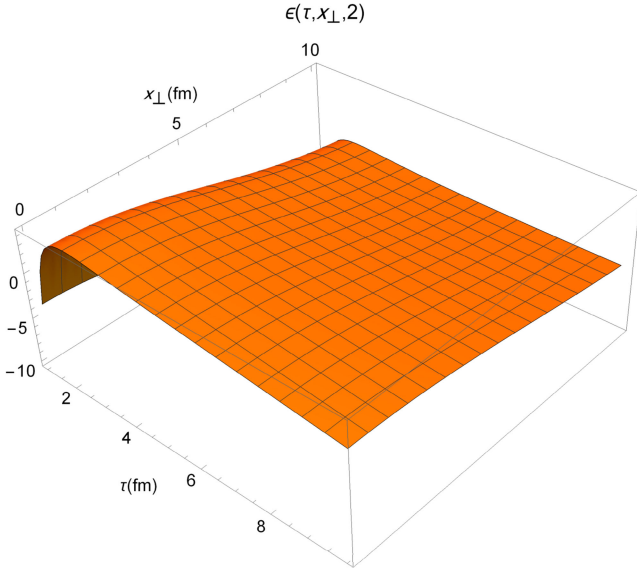


FIG. 11. $\epsilon(\tau, x_{\perp}, \eta)$. The values $A_1 = 0.3$, $A_2 = -0.07$, $q = 1/6.4 \text{ fm}^{-1}$, $\tau_0 = 1 \text{ fm}$, $\epsilon_c = 5.4$, and $\hat{\epsilon}_0 = 1500$ are chosen.

IV. CONCLUSION

In this study, we present a novel extension of Bjorken flow that accounts for a medium with finite transverse dimensions, which undergoes radial and axial expansion. Additionally, we explicitly consider the breaking of boost invariance, while preserving its fundamental characteristics. The conservation equations are solved analytically and perturbatively, leading to the derivation of a new set of exact solutions for the 1 + 2D ideal hydrodynamics. These solutions are capable of accurately describing heavy-ion collisions at finite collision energies. We provide a detailed analysis of the modifications to the fluid velocity and energy density resulting from our proposed approach.

The present study involves the identification of terms that are proportional up to the second order in λ_1 , resulting in a set of equations. However, the conservation equations have only been solved up to the first-order expansion, with the general solutions expressed in terms of a series. To obtain physical solutions, we impose the analytic conformal solutions discovered by Gubser [8] at $\tau = \tau_0$. The coefficients of the general solutions in transverse expansions are then determined through the utilization of the orthogonality of Bessel functions. In the longitudinal expansions, the constant coefficients A_0 , A_m , and B_m are determined based on physical conditions and some simplifications. It should be noted that knowledge of the flow rapidity profile $Y(\tau, \eta)$ at initial proper time τ_0 is necessary, but for simplicity, only the first two terms in Eq. (2.52) have been retained, representing the corrected flow rapidity solutions. Finally, utilizing a first-order perturbation expansion, we have derived the energy density, transverse flow velocity, and flow rapidity.

To investigate the expansion of flow in the transverse plane, we have opted to utilize the Gubser flow as our initial flow configuration. The transverse expansion of the quark-gluon plasma has been characterized by two parameters, specifically q and $\hat{\epsilon}_0$, which have been introduced by Gubser's solution. Our objective has been to explore the parameter space of these two parameters in order to identify suitable values that can accurately simulate heavy-ion collisions. It has been observed that selecting $\hat{\epsilon}_0 = 1500$ and $1/q = 6.4 \text{ fm}$ yields reasonable results. Additionally, a comparison has been conducted between the radial velocity and correction energy density obtained from our model and those obtained from the Gubser model. The findings indicate that the distribution of energy density in our model is comparatively smoother than that of the Gubser flow. Furthermore, we have evaluated the transverse flow velocity obtained from our model in relation to the phenomenological proposition of $v_{\perp} = \frac{x_{\perp}}{50}$. In fact, an alternative radial flow

profile has been employed at the initial proper time τ_0 , as investigated in the study conducted by [22], in order to calculate the coefficients c^k of our general solutions. Subsequently, a comparison has been made between the radial flows obtained from different initial conditions, namely the Gubser flow and the phenomenological proposal profiles. The results of our analysis have indicated that, when the value of q is set to $1/6.4 \text{ fm}^{-1}$ and $x_\perp < 5$, the radial velocities of systems with varying initial conditions tend to converge towards a common late-time behavior.

The present study focuses on investigating the longitudinal expansion of the flow in a particular model, which exhibits a partial breakdown of boost invariance in longitudinal expansion. The rapidity distribution of the energy density has been obtained through computations using a perturbative method. Our findings indicate that the rapidity distribution is approximately Gaussian, albeit with a broad shape. Consequently, the deviations from the Bjorken flow are not substantial. In order to analyze the overall characteristics of the flow, we also derived approximate solutions for

the acceleration parameter under the assumption of broad Gaussian distributions in the central region. To accomplish this, appropriate values for the free parameters A_1 and A_2 , which describe the expansion of the quark-gluon plasma in the longitudinal direction, have been selected.

In our analysis, we have adopted a perturbative approach to model the plasma, which is superimposed on the background flow, rather than conducting a comprehensive hydrodynamical calculation. The insignificance of the observed effects validates our methodology. However, we must emphasize that our calculations are based on several crucial assumptions; namely, we have considered the medium's two fundamental properties, assuming central collisions that lead to azimuth symmetry, a small transverse velocity compared to longitudinal expansion ($u_\perp \ll 1$), and a soft breakdown of boost invariance ($Y - \eta \ll 1$). Relaxing these assumptions could yield intriguing outcomes and warrant further investigation. Nonetheless, any deviation from these assumptions would render the calculation significantly more complex.

-
- [1] R. Andrade, F. Grassi, Y. Hama, T. Kodama, and O. Socolowski, Jr., On the necessity to include event-by-event fluctuations in experimental evaluation of elliptical flow, *Phys. Rev. Lett.* **97**, 202302 (2006).
 - [2] P. Romatschke and U. Romatschke, Viscosity information from relativistic nuclear collisions: How perfect is the fluid observed at RHIC?, *Phys. Rev. Lett.* **99**, 172301 (2007).
 - [3] H. Song and U. W. Heinz, Causal viscous hydrodynamics in $2 + 1$ dimensions for relativistic heavy-ion collisions, *Phys. Rev. C* **77**, 064901 (2008).
 - [4] P. Bozek, Flow and interferometry in $3 + 1$ dimensional viscous hydrodynamics, *Phys. Rev. C* **85**, 034901 (2012).
 - [5] C. Gale, S. Jeon, B. Schenke, P. Tribedy, and R. Venugopalan, Event-by-event anisotropic flow in heavy-ion collisions from combined Yang-Mills and viscous fluid dynamics, *Phys. Rev. Lett.* **110**, 012302 (2013).
 - [6] L. Del Zanna, V. Chandra, G. Inghirami, V. Rolando, A. Beraudo, A. De Pace, G. Pagliara, A. Drago, and F. Becattini, Relativistic viscous hydrodynamics for heavy-ion collisions with ECHO-QGP, *Eur. Phys. J. C* **73**, 2524 (2013).
 - [7] J. D. Bjorken, Highly relativistic nucleus–nucleus collisions: The central rapidity region, *Phys. Rev. D* **27**, 140 (1983).
 - [8] S. S. Gubser, Symmetry constraints on generalizations of Bjorken flow, *Phys. Rev. D* **82**, 085027 (2010).
 - [9] P. Staig and E. Shuryak, Fate of the initial state perturbations in heavy ion collisions. II. Glauber fluctuations and sounds, *Phys. Rev. C* **84**, 034908 (2011).
 - [10] P. Staig and E. Shuryak, Fate of the initial state perturbations in heavy ion collisions. III. The second act of hydrodynamics, *Phys. Rev. C* **84**, 044912 (2011).
 - [11] J. I. Kapusta, B. Müller, and M. Stephanov, Relativistic theory of hydrodynamic fluctuations with applications to heavy-ion collisions, *Phys. Rev. C* **85**, 054906 (2012).
 - [12] S. Shi, J. Liao, and P. Zhuang, “Ripples” on a relativistically expanding fluid, *Phys. Rev. C* **90**, 064912 (2014).
 - [13] T. Csorgo, M. I. Nagy, and M. Csanad, A new family of simple solutions of relativistic perfect fluid hydrodynamics, *Phys. Lett. B* **663**, 306 (2008).
 - [14] K. J. Eskola, K. Kajantie, and P. V. Ruuskanen, Hydrodynamics of nuclear collisions with initial conditions from perturbative QCD, *Eur. Phys. J. C* **1**, 627 (1998).
 - [15] P. Bozek and I. Wyskiel, Rapid hydrodynamic expansion in relativistic heavy-ion collisions, *Phys. Rev. C* **79**, 044916 (2009).
 - [16] P. Bozek, Viscous evolution of the rapidity distribution of matter created in relativistic heavy-ion collisions, *Phys. Rev. C* **77**, 034911 (2008).
 - [17] J. Ze-Feng, Y. Chun-Bin, Máté Csanád, and Tamás Csörgő, Accelerating hydrodynamic description of pseudorapidity density and initial energy density in $p + p$, $\text{Cu} + \text{Cu}$, $\text{Au} + \text{Au}$ and $\text{Pb} + \text{Pb}$ collisions at energies available at BNL relativistic heavy ion collider and the CERN Large Hadron Collider, *Phys. Rev. C* **97**, 064906 (2018).
 - [18] Shuzhe Shi, Sangyong Jeon, and Charles Gale, Family of new exact solutions for longitudinally expanding ideal fluids, *Phys. Rev. C* **105**, L021902 (2022).

- [19] M.I. Nagy, T. Csörgő, and M. Csanád, Detailed description of accelerating, simple solutions of relativistic perfect fluid hydrodynamics, *Phys. Rev. C* **77**, 024908 (2008).
- [20] T. Csörgő, M.I. Nagy, and M. Csanád, A new family of simple solutions of perfect fluid hydrodynamics, *Phys. Lett. B* **663**, 306 (2008).
- [21] K. Adcox *et al.* (PHENIX Collaboration), Formation of dense partonic matter in relativistic nucleus nucleus collisions at RHIC: Experimental evaluation by the PHENIX Collaboration, *Nucl. Phys.* **A757**, 184 (2005).
- [22] P.F. Kolb and R. Rapp, Transverse flow and hadrochemistry in Au + Au collisions at $\sqrt{s_{NN}} = 200$ GeV, *Phys. Rev. C* **67**, 044903 (2003).
- [23] U. Gürsoy, D. Kharzeev, and K. Rajagopal, Magnetohydrodynamics, charged currents and directed flow in heavy ion collisions, *Phys. Rev. C* **89**, 054905 (2014).